Electrical Power and Energy Systems 171 (2025) 111053

Contents lists available at ScienceDirect

International Journal of Electrical Power and Energy Systems

journal homepage: www.elsevier.com/locate/ijepes

Impedance-based Thermal Runaway early detection methodology for Lithium-Ion batteries

J. Perez [a,*], E. Garayalde [b], J. Lorente [a], M. Arrinda [a], M. Oyarbide [a], H. Macicior [a], U. Iraola [b], H.J. Grande [a,c]

[a] CIDETEC, Basque Research and Technology Alliance (BRTA), Po. Miramón 196, 20014 Donostia-San Sebastian, Spain
[b] Mondragon Unibertsitatea, Faculty of Engineering, Electronic and Computing Department, Loramendi 4, 20500 Mondragon, Gipuzkoa, Spain
[c] Advanced Polymers and Materials: Physics, Chemistry and Technology Department, University of the Basque Country (UPV/EHU), 20018 Donostia-San Sebastian, Spain

ARTICLE INFO

Keywords:
Lithium-ion batteries
Thermal Runaway
Electrochemical Impedance Spectroscopy
Battery safety
State of Safety

ABSTRACT

In this work, a new impedance-based Thermal Runaway (TR) early detection methodology for Li-ion batteries is proposed. By using Electrochemical Impedance Spectroscopy (EIS), the impedance of a battery has been tracked during a full TR event. The potential of EIS and cell impedance tracking for detecting a TR event in an early stage is demonstrated, thus improving battery safety and State-of-Safety estimation. The impedance module and phase trends are studied based on single-frequency impedance measurements to detect the event. To develop the impedance-based detection strategy, Accelerating Rate Calorimetry tests are carried out to characterize cell impedance behavior at different temperatures and different State-of-Charge values. This characterization is used to select the most adequate frequency range for detecting a TR event. Then, this methodology is validated by fast-paced (under 20 min) over temperature abuse tests, demonstrating that this methodology is valid for both rapid and slow-paced TR events. In addition to this, the performance of this methodology is compared to gas sensing based TR detection, using current State-of-the-Art automotive grade gas sensors for this purpose. The results show that the impedance-based method detects the TR 15 h before the explosion in a slow-paced event. The impedance-based method also outperforms the gas sensing based detection at fast-paced events, complying with regulations such as R100 Rev3 requirements of a 5-minute warning.

1. Introduction

Lithium-ion batteries (LIBs) have become a cornerstone of modern energy storage solutions due to their high energy density, long cycle life, and relatively low maintenance. They are widely used across various types of applications, from portable electronics and Electric Vehicles (EVs) to stationary applications with large-scale energy storage systems. In recent years, incidents involving lithium-ion batteries in EVs have captured significant public attention, raising widespread concern about their safety. A major risk associated with these batteries is Thermal Runaway (TR), where excessive heat can lead to fires or explosions. This has caused potential buyers to view the technology as less reliable and secure.

Thermal Runaway in LIBs is typically triggered by several factors, including mechanical abuse, electrical abuse, and thermal abuse. Mechanical abuse, such as crushing or puncturing, can damage internal components and lead to short circuits [1]. Electrical abuse, including over charging or over discharging, causes excessive heat generation due to the breakdown of battery materials and exothermic reactions [2,3]. Thermal abuse, where the battery is exposed to high external temperatures, can degrade the separator and lead to internal short-circuits. Extremely low temperatures can also be detrimental as they may lead to Lithium Plating, which in severe cases can form dendrites that penetrate the separator, potentially causing an internal short-circuit [4,5]. Regardless of the cause that generated the Thermal Runaway, the mechanisms behind it involve a close interaction between electrochemical and thermal processes within the battery. It first starts with the breakdown of the solid electrolyte interphase (SEI) layer on the anode, leading to reactions between the anode and the electrolyte. As the temperature rises, the electrolyte begins to decompose, releasing flammable gases. Simultaneously, the separator, which keeps the anode and cathode apart, can degrade or melt causing an internal short circuit.

* Corresponding author.
E-mail address: jonperez@cidetec.es (J. Perez).

https://doi.org/10.1016/j.ijepes.2025.111053
Received 8 April 2025; Received in revised form 3 August 2025; Accepted 21 August 2025
Available online 27 August 2025

Once the TR is initiated, the temperature rise accelerates increasing the internal pressure and generating more heat than the battery can dissipate. The rapid increase in temperature accelerates the chemical reactions, creating a feedback loop that leads to uncontrolled heat release, gas emissions, and in severe cases, fire or explosion.

Considering regulatory requirements among other factors, the selected TR detection method should meet certain key criteria. First, it must detect the event at least 5 min before it occurs. Additionally, the solution should be easy to implement, minimally invasive, and cost-effective. Lastly, the method should provide a high degree of reliability in detecting TR while minimizing the occurrence of false positives.

The selection of a proper early detection method is crucial for preventing catastrophic battery failures and improving battery safety. Besides, the TR early detection has become mandatory by regulatory standards such as R100 Rev3, GTR-EVS, GB 38031–2020 or IEC 62933–5-2 [6–9]. In particular, the R100 Rev3 standard specifies that the vehicle shall provide a signal to activate the advance warning indication in the vehicle to allow egress of 5 min prior to the presence of a hazardous situation inside the passenger compartment due to a TR event [6]. To do so, several different approaches for an early detection of TR have been proposed in the literature.

While different studies have demonstrated the effectiveness of these methods in detecting TR, only a limited number meet the industry standards for practical implementation [10]. Raghavan et al. studied the implementation of fiber-optic sensors for measuring the internal pressure of the battery [11,12]. Although the sensor was successfully integrated within the pouch cell and was well sealed, the high costs of the sensors plus the complex assembly process limit their usability. Several authors have studied the measurement and analysis of the expansion force from the gas generated during the internal side reactions of a TR event. The expansion force has been proven to be effective for early warning. Nevertheless, these sensors are also complex for assembly, their signal-to-noise ratio decreases their reliability and cannot be implemented in cylindrical cell monitoring [13,14]. Furthermore, due to the gas release from the cell in a specified volume (the battery pack), the pressure is also believed to be useful for gassing and TR detection. In this regard, Koch et al. [15] carried out abusive tests to some State-of-the-Art automotive NMC pouch cells with the objective of comparing the time response of many sensors for TR detection. During the overheating abusive test, the pressure sensor was able to detect a pressure rise a few seconds before a visible venting on the cell. However, during nail penetration tests, the pressure sensor had almost no variation. The authors also proved that the gas sensors were able to detect the TR event far before the pressure sensor could. In addition, in the research carried out by Essl et al. [16], the pressure sensor used in their abusive tests was not able to detect the first venting of the cell at all. Appleberry et al. and Bombik et al. analyzed the feasibility of employing ultrasound-based TR detection, by measuring the Time-of-Flight through the layers of the cell. Ultrasound provides high sensitivity and reliability for this purpose, but up to date, this approach is only applicable to pouch cells with small capacity [17,18]. Other authors have tackled the detection of TR through the monitoring of the internal cell temperature with embedded sensors within the cell [19,20]. In previous studies, the potential lag between internally and externally measured cell temperature has been demonstrated [19,21], so directly sensing the internal cell temperature definitely improves the TR detection capabilities. However, the assembly of these embedded sensors is costly, it is not standardized, and many employed sensors have received interferences depending on the application, decreasing their reliability. Su et al. and Lyu et al. have analyzed the measurement of the acoustic signal from the cell venting for early warning. The authors successfully detected the event before voltage or surface temperature warnings, but this approach also requires complex mechanical integration due to the needed proximity to the cell, and suffers from noise, especially in EV environments [22,23].

On the other hand, gas sensors are a promising solution, since only one sensor would be needed per battery pack ideally, which makes their implementation much simpler than other methods. The main challenge or limitation is the choice of the type of sensor depending on the gas to be measured. Depending on the type of battery (NMC, LFP, LTO, …) and the phase of the TR, different types of gases are released, so a specific sensor is needed for their detection [24,25]. Electrochemical Impedance Spectroscopy (EIS) also offers a viable alternative, with recent advances in chip-level impedance measurements enabling integration into BMS [26]. The integration of a single chip in the BMS would be enough to perform multiplexed impedance measurements of each of the cells within the battery module, making it a cost-effective and minimally invasive solution. While conventional EIS measurements take several minutes to complete, limiting its effectiveness for TR detection, single-frequency impedance evaluation has been proposed in several research articles as a faster alternative [27–29]. There is a growing body of research exploring the use of full-spectrum and single-frequency EIS applied to battery diagnostics, including State-of-Health (SoH) estimation, State-of-Charge (SoC) estimation or Lithium Plating detection [30–34]. Despite this, the selection process of the best frequency for this analysis is not clear. Spinner et al. used 300 Hz for the analysis, but did not describe why they chose this frequency [27]. Raijmakers et al. used the intercept frequency (f_0) because of its SoC independency, but this frequency was not necessarily the one with the most temperature dependency [28]. Srinivasan et al. used measurements at 10 Hz and 70 Hz, both fixed by the BMS capabilities [35]. Dong et al. selected 31.62 Hz to analyze the cell temperature, but it is unclear why this is the optimal frequency for this purpose [36]. As for the frequency selection for other battery diagnostics, some use DRT analysis for this purpose. While DRT analysis provides a detailed view of the electrochemical processes, helpful for selecting the frequencies at which the target process takes place, it requires interpretation and good understanding of the DRT and the battery's electrochemical processes.

Overall, considering the integration of EIS and gas sensors into real electric mobility applications for TR detection purposes, both solutions would meet all the previously mentioned requirements. These techniques are easy to implement, minimally invasive, and economically viable, making them suitable for both new battery-pack designs and retrofitting existing packs with little to no modification of the battery's mechanical components.

This study proposes a methodology based on impedance measurement TR detection to effectively increase the detection time of TR, improving overall battery safety and contributing to a State-of-Safety (SoS) estimation. Furthermore, this method uses single-frequency impedance measurements, so this technique can be applied with a single EIS measurement IC for every cell within the module. This contributes to the feasibility of introducing these measurements in the BMS. In addition, the proposed impedance-based methodology is compared to gas-sensor based TR detection to quantify the potential improvements of employing EIS measurements in a BMS. The developed impedance-based TR detection methodology on its own introduces several advancements and novelty beyond the current State-of-the-Art. (i) A framework for selecting the optimum frequency for analysis is proposed. (ii) The TR detection methodology is compared to commercial gas sensors for TR detection, and it is validated at different TR scenarios: fast event, slow event, at cell level and at module level. (iii) This methodology complies with the current 5-minute warning limit specified in regulations, such as the UN ECE R100 Rev 3.

The rest of this paper is organized as follows: Section 2 lays the foundation and background of how impedance measurements and gas sensors are applied to detect a Thermal Runaway. In addition, the test setup and the impedance-based TR early warning strategy are described. Section 3 shows the test results, describing them and comparing impedance-based and gas sensor-based TR detection approaches. In Section 4, the main findings of this work and future lines for study are laid out.

2. Methodology

In this section, the background behind gas-based and impedance-based TR detection is described. Then, the experiments carried out, the Device Under Test (DUT) and the impedance-based warning strategy are described.

2.1. Gas sensing applied to Thermal Runaway detection

During the Thermal Runaway process, many different gases are released. Hence, gas sensing technology can contribute to an early warning of the event. Depending on the TR event stage, different side-reactions and material decomposition take place, thus different gases will be released. There is much research available in the literature studying the composition of the gases released from different cell chemistries. The decomposition of the SEI layer is one of the first stages during a Thermal Runaway event. At this point, when the SEI starts decomposing, CO_2 is mainly released [37]. Once the SEI breaks, the electrolyte will start to react with the anode and CO, H_2 and HF will be released [24]. In addition to this, at this point, the low-boiling solvents of the electrolyte will start to evaporate [25]. Depending on the electrolyte used, Volatile Organic Compounds (VOC) such as DMC (91 °C), DEC (126 °C) or EMC (110 °C) will also be released. Then, when the first venting takes place, apart from the VOCs coming from the electrolyte vaporization, CO and CO_2 will also be released. Up to this point, the gases produced during the TR event are not dependent on the cathode chemistry used, but instead, they are dominated by the used electrolyte mixture [16]. Finally, if the TR is reached, the cathode material used in the cell will determine the gas concentrations released, but mainly, the released gases at this stage are CO, CO_2 and H_2. In this part, the thermal stability of the cathode, the decomposition temperatures and the oxygen release are of paramount importance [38]. Although CO_2 release begins in the first stage of a TR event, its low concentration makes it hard to detect it at this stage. For an early detection of a TR event, it has been discovered that electrolyte vapors are the most useful for their high concentration at an early stage of a TR. Furthermore, VOC depends on the electrolyte mixture rather than cathode composition, hence VOC sensitive sensors are very interesting for this purpose.

2.2. Impedance measurements applied to Thermal Runaway detection

EIS is a powerful, relatively fast, non-invasive technique used for impedance analysis in electrochemical systems which provides insight into various electrochemical processes occurring at different frequencies. Each electrochemical process in a lithium-ion battery has its own time-constant, hence, they can be characterized over a range of frequencies. For lithium-ion batteries, EIS is mainly used for cell electric and electrochemical characterization and modeling purposes. However, recently the EIS method has gained importance in the literature for diagnosis of internal status of the battery cells, such as internal temperature estimation or aging detection [39,40].

EIS is employed in this study due to the impedance's sensitivity to changes in battery internal processes that occur during a Thermal Runaway event. The methodology aims to leverage these changes in impedance for early detection, specifically focusing on temperature variations. This approach provides a more effective solution compared to existing methods such as gas sensing, which may have delayed responses depending on their location [16].

The SoC and temperature dependency of the impedance of a battery has been already widely studied in literature, and since the impedance is also dependent on the frequency, changes are also observed in the impedance spectra. Regarding the temperature dependency of the impedance, it is determined mostly by the cell material characteristics [41]. This dependency is evident in the whole frequency range of the EIS, but it is most sensitive in the intermediate-low frequency region, while at high frequencies (inductive area) the temperature effect is not that great. On the other hand, SoC dependency of the impedance changes deeply depending on the frequency. At low frequencies, in the diffusion and charge transfer process area, a strong deviation in the impedance is observed for different SoC [28,41]. For a sufficiently high frequency, the SoC effect on the impedance can be neglected [42]. The SEI layer, since it does not store any charge within it, its impedance is insensitive to SoC and the charge-transfer resistance. So, if a stable SEI exists, a temperature dependency will be observed in the SEI [27,35]. The frequency where the SoC effect can be neglected depends on the battery cell and varies in each study. For instance, very little SoC effect is observed above 6 Hz in the study carried out by Zhu et al. [43], while in [27,35,36] this frequency rises to 10 Hz, 30 Hz and 100 Hz respectively. This temperature and SoC dependency form the basis of the early detection strategy presented in this work.

For higher working temperatures, the cell impedance is known to decrease. However, for a sufficiently high temperature, the cell impedance has been demonstrated to increase substantially, instead of decreasing [25]. The reason behind this behavior is not clear yet and could be caused by different events, some authors have provided some hypotheses, such as severe depletion of the electrolyte or separator shutdown process among others [25]. Focusing on the impedance tendency for high temperatures, it has been noted that the phase shift of the impedance shows quite an interesting behavior. Dong et al. [36] demonstrated in their research that past a certain temperature, the phase of the impedance converged to a certain value and would remain so for higher temperatures. Srinivasan et al. [35] achieved the same results in their study, although they further observed that moments before the venting, the phase shift recovered to a more normal value, indicating that the cell was being cooled due to the gas generation and posterior venting. While the SoC and temperature effects on impedance have been well-studied in previous works, the present study expands upon these findings by focusing on their role in detecting Thermal Runaway conditions.

2.3. Device under test and experiment setup

Commercial *Samsung* INR21700-50E cylindrical lithium-ion cells with a nickel–cobalt-aluminum oxide (NCA) cathode and a graphite anode were used in this study. The cells had a nominal capacity of 4.9 Ah. In Table 1, the general characteristics of the DUT are depicted. Prior to testing, the cells were activated with three charge and discharge cycles from 0 % SoC to 100 % SoC at a C/2 rate to ensure consistency in performance. All cells were then charged to the SoC required for the test at 25 °C and at least 24 h prior to the experiments. EIS was used to monitor the cell impedance throughout the Thermal Runaway events. EIS measurements were conducted using a *Gamry Interface 5000E* in a frequency range of 1 Hz to 1.6 kHz, with 50 mA of amplitude.

For the methodology proposed in this work, it is necessary to characterize the cell impedance during the Thermal Runaway. As explained in Section 2.2, both the SoC and the temperature influence the cell impedance, thus, it is of paramount importance that the impedance is

Table 1
Samsung INR21700-50E cell characteristics.

Parameter	Value
Nominal voltage (V_n)	3.6 V
Minimum voltage (V_{min})	2.5 V
Maximum voltage (V_{max})	4.2 V
Nominal capacity (C_n)	4900 mAh
Charging current (I_{cc})	C/2 (1C max.)
Discharging current (I_{dc})	2C (3C max.)
Charging temperature (T_{cc})	0 to 45 °C
Discharging temperature (T_{dc})	−20 to 60 °C
Cathode material	Li(NiCoAl)O2
Anode material	Graphite + 1 %wt Si
Mass	69.5 g

characterized at different SoC and temperature values. Furthermore, to ensure that the impedance measurement is accurate, the cell must be stationary at the required conditions. Hence, for performing the characterization of the impedance at these conditions, Accelerating Rate Calorimetry (ARC) tests were carried out in a THT EV + ARC calorimeter. The Heat-Wait-Seek (HWS) test protocol was followed, with a step of 5 °C, a waiting time of 30 min and a temperature rate sensitivity of 0.02 °C/min. ARC tests were conducted at 10 %, 50 % and 100 % SoC respectively. During the ARC tests, EIS measurements were performed at the end of the waiting period at each temperature, to ensure that the temperature was homogeneous throughout the cell. The tests were initialized at 25 °C and ended with the Thermal Runaway of the cells. Hence, the cell impedance has been characterized for three SoC values (10 %, 50 % and 100 %) and temperatures ranging from 25 °C up to 120 °C, where the cell voltage dropped, and EIS measurements could not be performed anymore. With this data, the methodology for the early detection of the Thermal Runaway is developed. This methodology is detailed in section 2.4.

ARC testing provides the perfect framework for characterizing the impedance at different SoC and temperature values, but it is a use case that most likely will just take place in a laboratory. Furthermore, the gas sensors cannot be placed in the calorimeter, since the maximum operating temperature of the electronics is exceeded. For properly validating the methodology and comparing the results to the sensors, tests are conducted under harsher, real-world conditions using overtemperature as a TR trigger. Hence, to validate the effectiveness of these approaches, overtemperature tests were performed in the abuse chamber. The heater is attached to the cell with metallic cable ties, and the cell is hung in the center of the chamber, for limiting the heat conduction losses. 3 thermocouples were used for tracking the cell's temperature, on the positive tab, on the negative tab and on the cell center. The overtemperature test setup is shown in Fig. 1. The cells were heated continuously, without a waiting period, with a heater dummy cell, at a constant power of 80 W until the Thermal Runaway was triggered. Two tests were carried out, one at 100 % SoC and another one at 50 % SoC. The most important feature of these tests is that a fast-paced Thermal Runaway is triggered, taking under 20 min from the beginning of the test. The ARC tests were more than 30 h long for reference. Hence, a more restrictive use case is considered for validation.

EIS measurements at the selected frequency (more details in Section 2.4) were performed continuously to track the impedance changes during the TR at this specific frequency and detect the onset of the TR. To benchmark the performance of this impedance-based method, automotive-grade sensors for TR detection were placed within the abuse chamber. The selected sensor is the BAS6C-X00 from Honeywell. This sensor targets aerosol particles, which are also sensitive to VOC. VOCs are released during the first stages of the TR. The sensor data is published over a CAN bus for monitoring.

Finally, for analyzing the capabilities of each detection method at a greater scale, an 8-cell battery module in an 8s1p configuration is tested (see Fig. 2). Here, a dummy cell with a heater inside is placed in the middle of the module, thus triggering the TR due to overtemperature to two cells almost at the same time. In this test, the capabilities of the analyzed methods for detection of a TR are analyzed at a module/pack level, demonstrating the benefits of applying redundancy to this detection. The EIS measurements were only applied to the cell closer to the heater. A summary of all the tests and their purpose is shown in Table 2.

2.4. Impedance-based Thermal Runaway early detection methodology

In the proposed methodology for early detection of TR in Li-ion batteries, frequency selection plays a critical role in ensuring the effectiveness of the EIS measurements. The impedance spectra, represented as a Nyquist plot, showed significant temperature-dependent behavior in the ARC tests, with the impedance initially decreasing as temperature increased, then reversing direction and increasing at approximately 90 °C (see Fig. 3). This inflection point is hypothesized to be linked to electrolyte vaporization and decomposition of the Solid Electrolyte Interphase (SEI) layer, both of which occur as the cell approaches hazardous thermal conditions. This behavior was particularly noticeable in the 100 % SoC test, where the impedance increased beyond 90 °C. More about this will be discussed in Section 3.

To optimize the methodology for early TR detection, a single-frequency approach is adopted to enhance the practicality of real-time monitoring. A full impedance spectrum can take several minutes to complete, making it unsuitable for rapid or real-world applications. By focusing on a specific frequency, a faster detection can be achieved at cell level, while also enabling the monitoring of every cell within a battery module with a single EIS device.

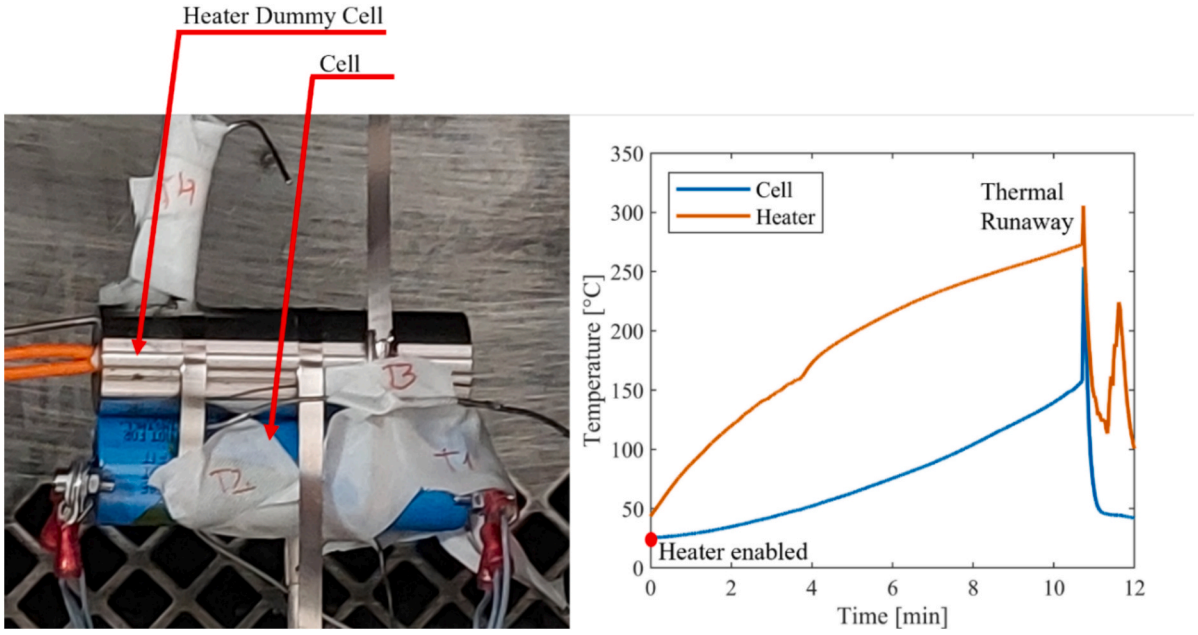

Fig. 1. Overtemperature test setup at cell level and temperature profiles of the test for cell and heater.

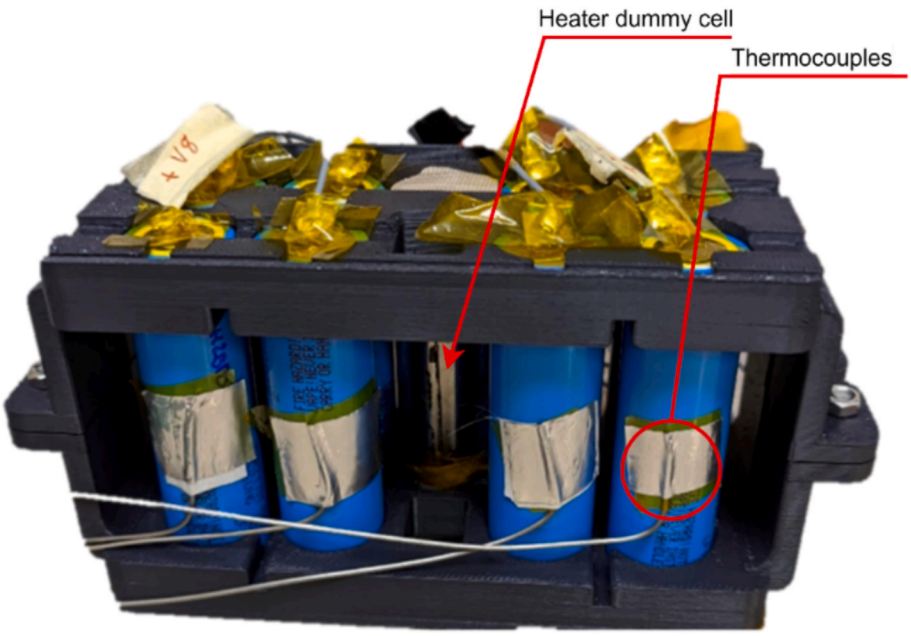

Fig. 2. 8-cell battery module for the overtemperature test at module level.

Table 2
Summary of the test matrix.

Test No.	Test type	SoC	Level	Objective
1	ARC	100 %	Cell	Characterize the cell impedance for different temperatures at 100 % SoC.
2	ARC	50 %	Cell	Characterize the cell impedance for different temperatures at 50 % SoC.
3	ARC	10 %	Cell	Characterize the cell impedance for different temperatures at 10 % SoC.
4	OVT	100 %	Cell	Validation of EIS detection method and comparison with commercial sensors at 100 % SoC.
5	OVT	50 %	Cell	Validation of EIS detection method and comparison with commercial sensors at 50 % SoC.
6	OVT	100 %	Module	Analysis of the performance of EIS and commercial sensors and comparison between them at fully charged module level.

2.4.1. *Frequency analysis*

For selecting the most appropriate frequency for this task, a frequential analysis of the impedance's parameters, namely, magnitude and phase, must be carried out. In Fig. 4, the impedance evolution depending on the SoC level and the cell temperature is shown. The cell impedance has great dependency for both SoC and temperature [35,36]. Hence, for selecting the final frequency, the objectives shall be to maximize the temperature effect while the SoC effect is reduced or minimized at that specific frequency. For this task, the statistical variance of each frequency to SoC and temperature, both for the phase and the magnitude, has been analyzed (see Fig. 5).

From the frequential analysis, several key takeaways can be obtained. Both the phase shift and the magnitude show dependency on temperature. However, the phase shift is the one which shows greater variability in its value due to temperature. In addition, the magnitude has greater dependency on SoC than on temperature, whereas the phase shift shows great dependency on temperature, whilst keeping SoC effect relatively low. Hence, the impedance phase shift is regarded to be the most suitable for tracking internal temperature changes. Focusing on the phase shift, at lower frequencies, the SoC effect is negligible, but so is the temperature effect. On higher frequencies however, the temperature effect is increased. At this region, the SoC effect is also increased, but it is kept low whatsoever. More specifically, the temperature dependency is observed to be greater for frequencies between 300 Hz and 1 kHz. This frequency range is where the SEI has greater weight in the impedance [27]. As previously discussed, the objectives for the frequency selection are: (i) maximize the temperature effect; (ii) minimize the SoC effect. For selecting the frequency objectively, it must be chosen numerically. The proposed approach for its selection is described in equation (1), where the temperature variance is multiplied by the inverse of the SoC variance. This way, the greater the temperature variance, and the smaller the SoC variance is, the obtained score for that frequency will increase. The scores of the frequencies in the range of 300 Hz to 1 kHz is shown in Table 3, ordered from highest to lowest score. The frequency with the greater score is 400.15 Hz, hence this frequency is selected as the best one for tracking the Thermal Runaway.

$$f_{score} = \sigma^2_{temp} / \sigma^2_{SoC} \tag{1}$$

Once the frequency is selected, further observations are made regarding the behavior of the phase shift with temperature at this frequency. As per Fig. 4, it is observed that the impedance phase showed substantial changes in the early stages of temperature increase. The variation in phase shift is particularly significant between 25 °C and the 48 °C measurement. At this temperature, the cell is approaching hazardous conditions, where the safety limits of the battery are going to be overcome. At temperatures above 60 °C, the SEI layer may start decomposing, being this the first exothermic reaction during a TR event. As the SEI layer decomposes, the graphite anode can be exposed to the electrolyte, and so the intercalated lithium in the anode can react with the electrolyte, causing loss of active material, lithium consumption and electrolyte consumption [24,44,45]. At this point, the low boiling-point solvents of the electrolyte will start to evaporate [46]. Furthermore, the Safety Operating Area (SOA) of this cell is exceed at this temperature (45 °C for charging). Interestingly, above 50 °C, the phase shift converges to the same value, with little variation from this point up to TR. As it will be demonstrated in the fast events in Section 3, this will prove to be useful for giving a first warning. For elevated temperatures both semi-circles of the impedance grow together and cannot be distinguished anymore. That means the time constants of the internal processes get similar and a separation is not possible anymore [47].

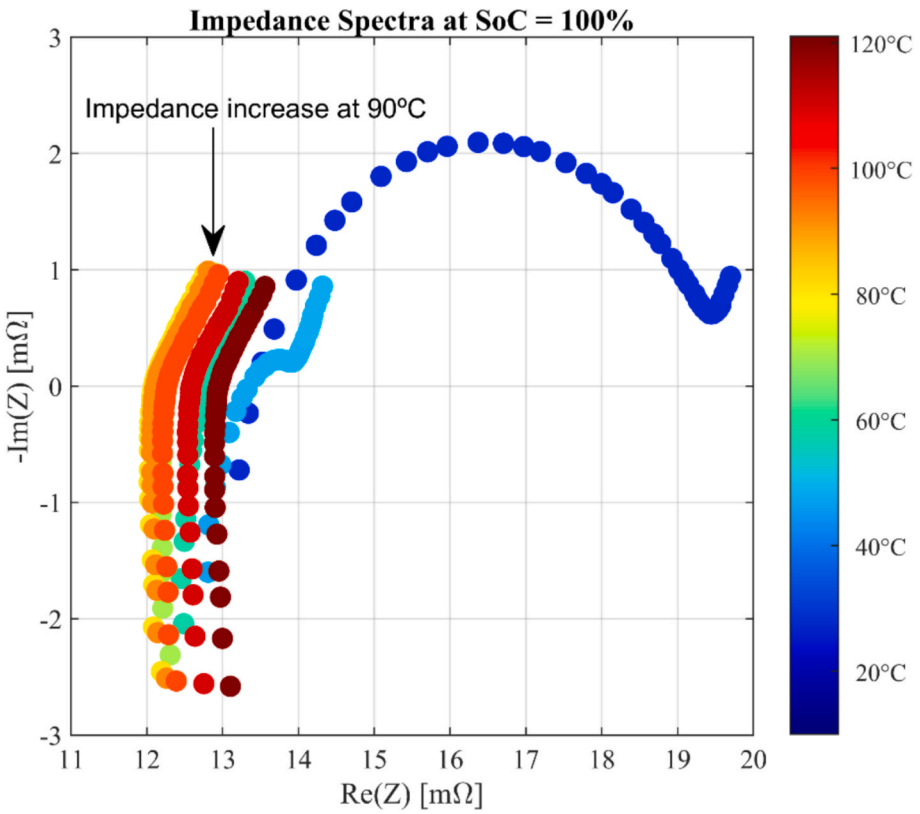

Fig. 3. Nyquist plot from room temperature up to Thermal Runaway. Test No. 1, 100% SoC ARC test.

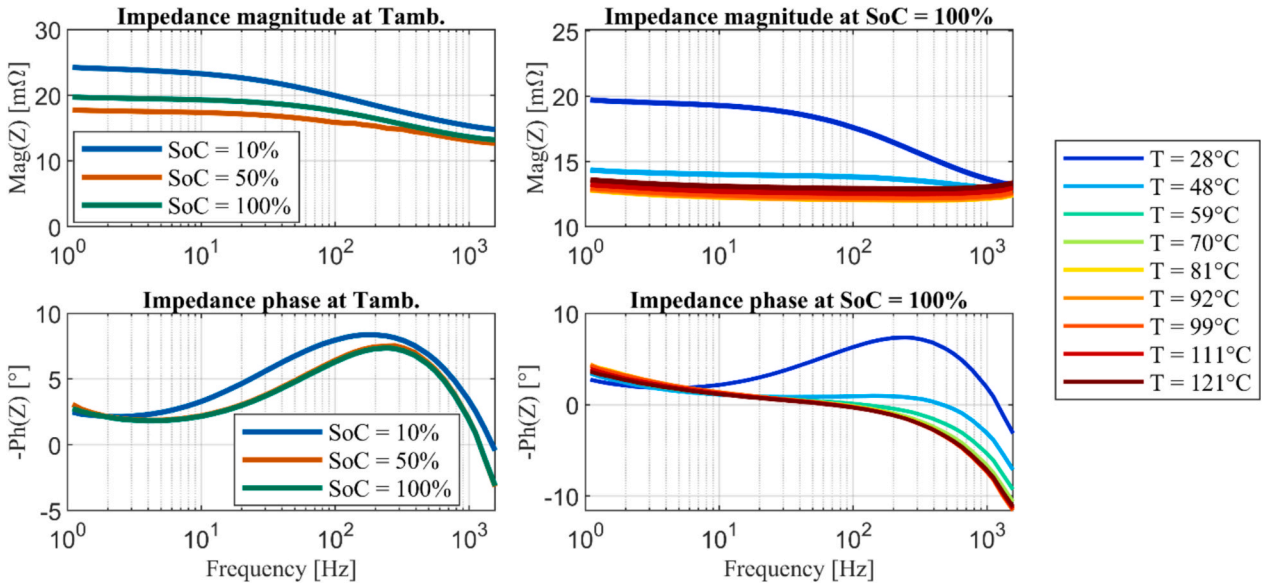

Fig. 4. SoC and temperature effect on each frequency during the ARC tests. Tests No. 1,2,3. 100 %, 50 % and 10 % ARC tests. SoC effect is analyzed on the impedance's magnitude and phase at ambient temperature, 25 °C. Temperature effect is analyzed from ambient temperature up to Thermal Runaway at 100 % SoC.

Increasing temperatures make the SEI layer behave more as a resistive layer rather than capacitive. This behavior suggests that at elevated temperatures, ionic conduction contributes to most of the current across the SEI layer [48].

Although this study is focused on TR events induced by thermal abuse, the proposed impedance based detection framework could potentially be extendend to other abuse scenarios, such as mechanical crush, external short circuit, internal short circuit and Lithium Plating. Previous studies have shown that these failure modes typically affect the impedance response at lower frequencies (difussion region) [49–51]. Since the selected frequency targets the SEI related processes (intermediate frequencies), the frequency for analysis would remain suitable for detecting the TR and would not need to be modified to account for these other abuse mechanisms.

2.4.2. *Impedance evolution and early warning system*

The impedance evolution at this frequency has been tracked over time during the ARC tests at the selected 400.15 Hz frequency. As

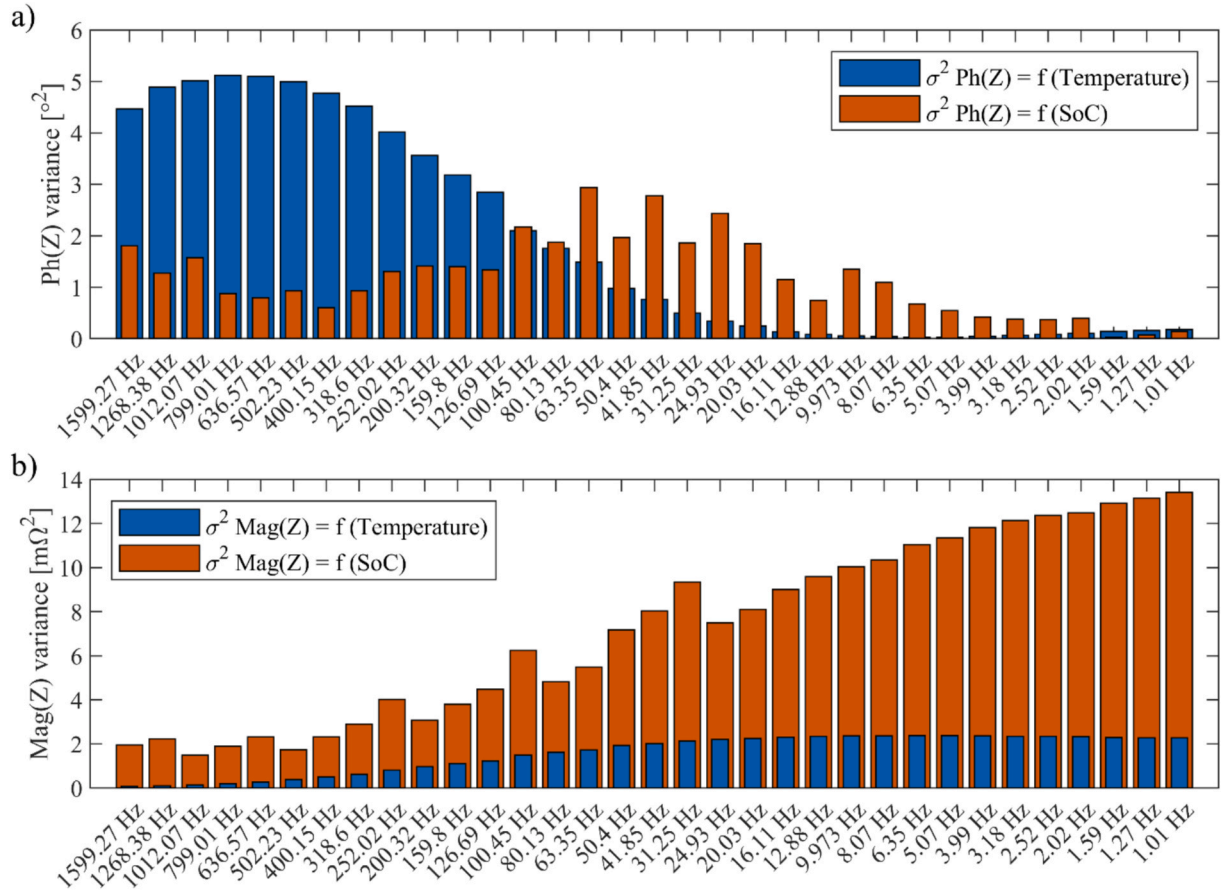

Fig. 5. A) impedance phase shift variance with temperature and soc at each frequency during the arc tests. b) impedance magnitude variance with temperature and soc at each frequency during the arc tests. tests no.1,2,3. 100%, 50% and 10% SoC ARC tests. Temperature effect is analyzed at Test No. 1, 100% SoC ARC test. SoC effect is analyzed at ambient temperature, from Tests No. 1,2,3, 100% SoC, 50% SoC and 10% SoC ARC tests.

Table 3
Frequency score values for selecting the optimum frequency, ordered from highest to lowest score.

Frequency	$\sigma^2_{temp}(\circ^2)$	$\sigma^2_{SoC}(\%^2)$	f_{score}
400,15 Hz	4,77	0,600	7,95
636,57 Hz	5,10	0,796	6,41
799,01 Hz	5,12	0,878	5,84
502,23 Hz	4,99	0,929	5,37
318,60 Hz	4,52	0,933	4,84

aforementioned in the frequential analysis, the phase shift exceeds −0.5° for temperatures above 50 °C approximately. Hence, the threshold of −0.5° is taken as reference for giving the impedance warning, where hazardous temperatures are exceeded. When three consecutive samples are taken below this threshold, a warning flag is raised. Furthermore, from the Nyquist plot (Fig. 3), it is observed that the impedance begins to increase at a cell temperature of 90 °C. The single-frequency measurements at the ARC tests revealed that at this temperature, the impedance magnitude and phase shift tendency decoupled from each other (see Fig. 6). This decoupling is a critical indicator, caused by the electrolyte vaporization and decomposition of other cell components, as stated in the beginning of chapter 2.4. This behavior signifies that the cell has entered a phase where the risk of TR increases significantly. The beginning of this decoupling is taken as the second warning point. Within a 1 min window, a phase shift variation under 0.2 % (based on the results from test No. 1) and the continuous increase of the magnitude (derivative greater than 0) within that time window are taken as reference for detecting this decoupling behavior. Likewise, after three consecutive samples are taken which fulfill those conditions, the second warning flag is raised. For the sake of consistency, this same criteria has been applied to all the abusive tests presented in this work. It must be noted that the frequency is cell specific, it is not universal. Although applying the same frequency to every cell could still be valid for TR detection, for achieving the best possible detection time each cell model must be characterized as shown in Section 2.4.1.

Taking all of the above into consideration, in the ARC tests, the first impedance warning, which takes into account the value of the phase shift, takes place almost 17.4 h and 18.9 h before the venting and the TR respectively. Regarding the second and last impedance warning, it happens at 13.79 h and 15.28 h before the venting and the TR respectively. As for the characteristic drop in voltage which usually takes place in such events, it is 9.81 h before the TR. In this type of slow events, considering that current BMS could only give a warning due to the undervoltage, the impedance warning system is able to raise an alarm more than 5 h before current BMS, which is a significant improvement.

As previously stated, gas sensors measuring VOC concentrations are employed to compare the effectiveness of the impedance-based TR detection in overtemperature tests. The VOC sensor has not been used during the ARC tests due to the high ambient temperatures during the test, which would not withstand such working temperatures. For the sake of consistency, the same criteria have been applied to all abusive tests to raise the warning by gas concentration. In total, two warnings are given, one based on the gas concentration increase over a given period of time, and another based on a threshold concentration value. Based on previous experience, the gas concentration increase rate for the used sensor is set at 300 $\mu g/m^3$ per minute. As for the threshold, the recommended value by the manufacturer is employed, 5000 $\mu g/m^3$.

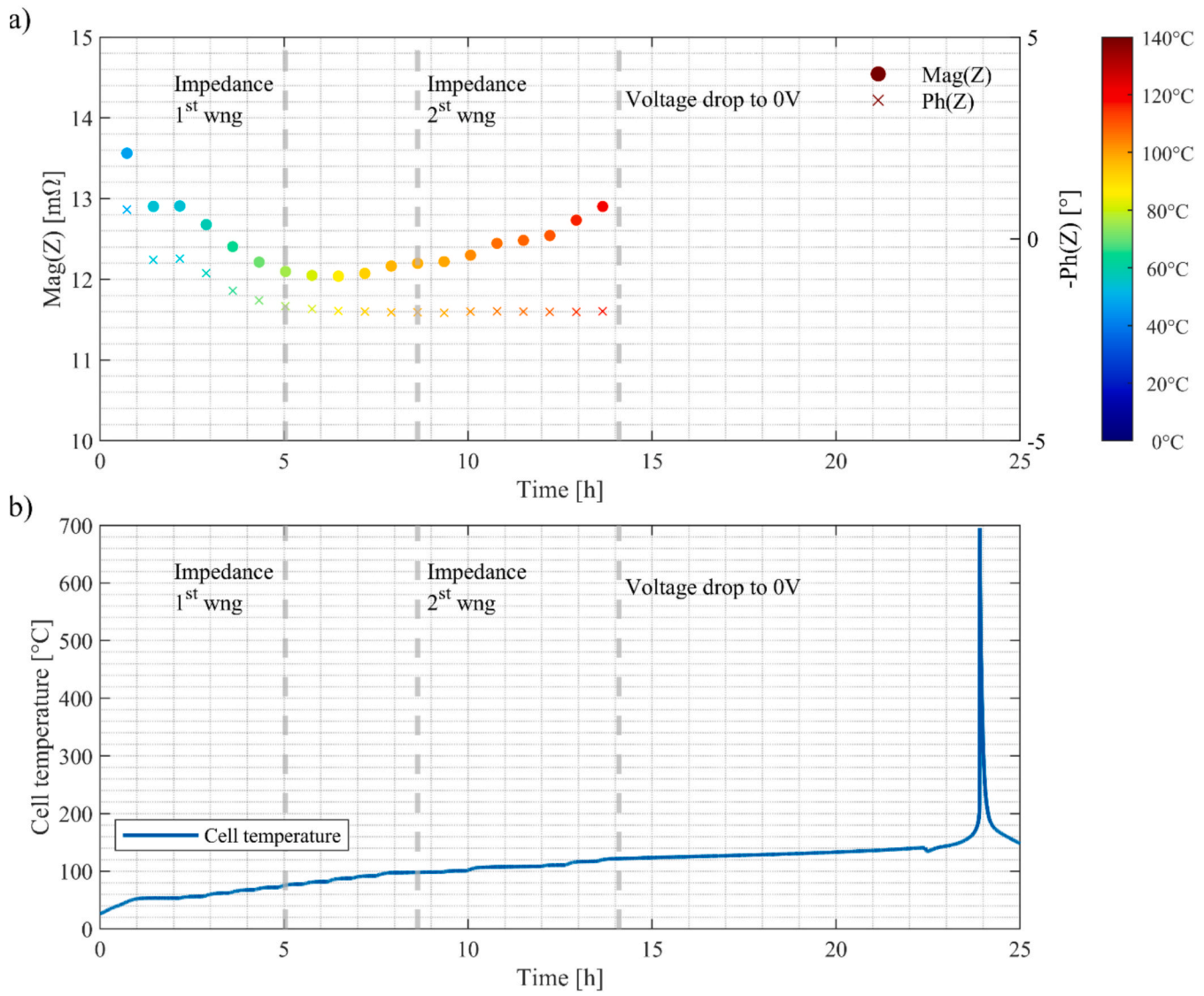

Fig. 6. A) impedance magnitude and phase evolution over time at the selected frequency of 400.15 Hz. b) Cell temperature evolution up to Thermal Runaway. Test No. 1, 100 % SoC ARC test.

3. Results and discussion

Once the impedance has been characterized with the ARC tests and the target frequency of 400.15 Hz has been selected for tracking the TR, the performance of this methodology in harsher, much faster TR events is tested and validated. For this task, two tests were carried out at 100 % SoC and 50 % SoC respectively. The 100 % SoC test was selected for being the worst-case scenario, where the cell has the maximum energy stored and the TR event is the harshest. As for the 50 % SoC test, this SoC level was selected to validate the proposed methodology in an intermediate SoC level, to analyze how both detection methods perform at different SoC levels. Finally, both detection methods are analyzed at system level by triggering TR to an 8-cell module. As previously discussed, during these tests, the cell impedance is continuously monitored at the selected frequency. Furthermore, automotive-grade gas sensors, targeting VOC are used to correlate impedance measurements to the cell's internal reactions and perform a comparison between the effectiveness of these detection methods.

3.1. 100 % SoC results

Following the TR warning criteria described in section 2.4.2, at the 100 % SoC fast event, the impedance phase dropped below −0.5° when the cell temperature exceeded 50 °C (see Fig. 7). This temperature is usually the safety limit set in the datasheet by cell manufacturers. Following the impedance-based warning criteria, 3 consecutive samples below this phase threshold are considered for giving the first warning, which is given at 54 °C cell temperature, 6.58 min before the TR. The impedance phase continuously decreased, stabilizing its value at −1.55° to −1.6° at 75 °C. This phase shift behavior was also observed in [35,36,43]. As for the impedance magnitude, it decreases with rising temperature until reaching the minimum value at 77 °C, similarly to the phase stabilization temperature. The second impedance warning, which comprises the increasing of the impedance magnitude while the phase value is stabilized, is given at 99 °C cell temperature, 3.08 min before the TR. Regarding the gas sensor, it starts measuring a concentration increase at 81 °C cell temperature. This gas sensor is sensitive to VOC, which are released when the electrolyte starts to evaporate. At this point, the impedance magnitude of the cell had already started to increase. This behavior is expected as it has been stated in Section 2.2. Research has shown that depending on the electrolyte used, VOC such as DMC can start evaporating at temperatures of 91 °C [25]. Hence, given the fast nature of the event, and considering the possible delay between the internal cell temperature and the outer body cell temperature

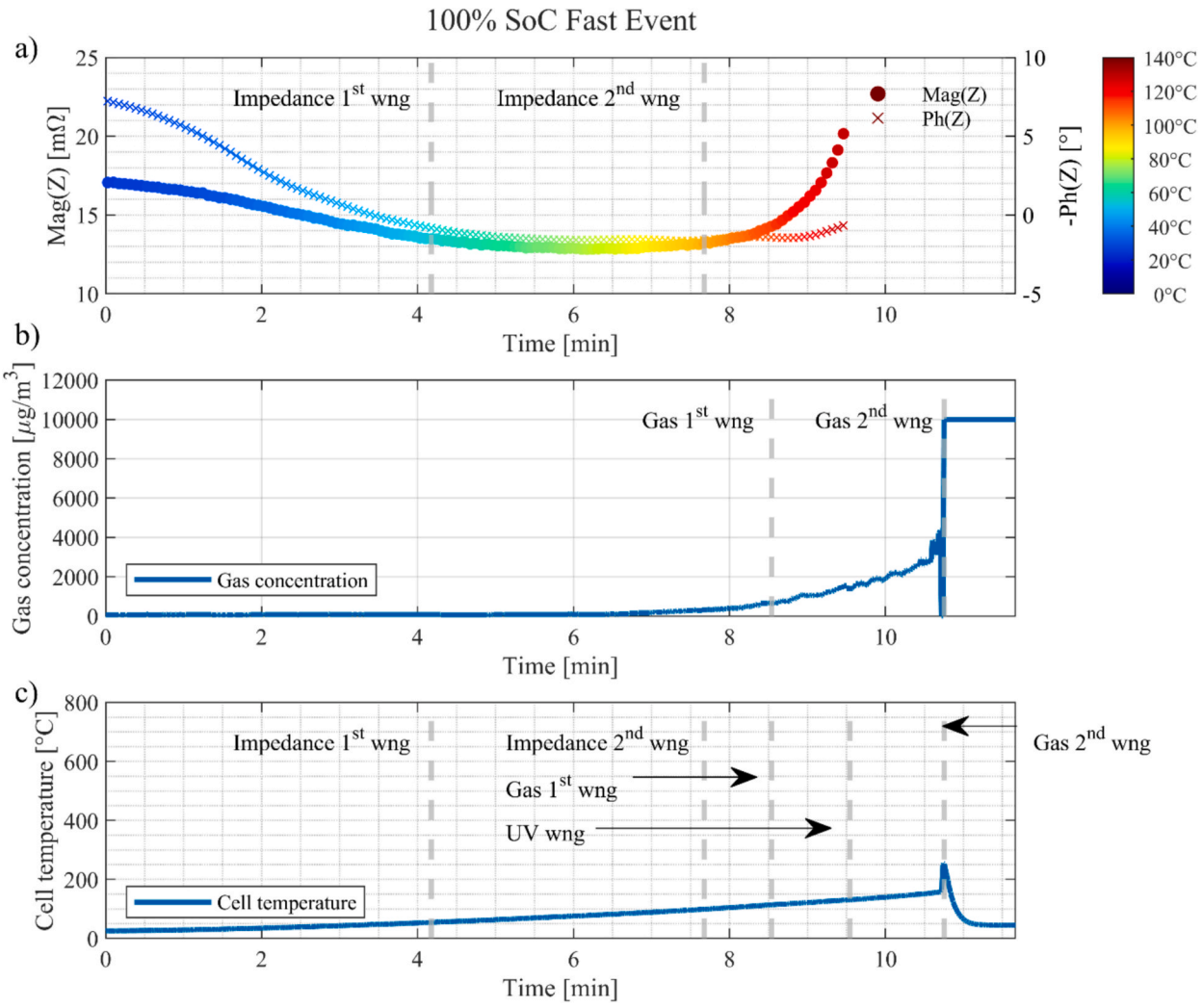

Fig. 7. Fast event results at Test No. 4, 100% SoC OVT test. a) Impedance magnitude and phase evolution over time at the selected frequency. b) Gas concentration evolution. c) Cell temperature evolution during the Thermal Runaway.

measured with thermocouples, it is reasonable to correlate the gas concentration, and the impedance increase to the electrolyte vaporization. Following the gas warning criteria, the first warning (concentration increase rate) is given at 2.21 min before the TR, while the second warning (concentration threshold) is not given until the explosion. On the other hand, the undervoltage warning is given 1.21 min before the explosion, a minute before the gas sensor's first warning. The low peak temperature value is caused by the thermocouple becoming loose due to the explosion.

3.2. 50 % SoC results

At the 50 % SoC fast event TR, the same trend in the impedance as in the 100 % SoC event is observed, although both the phase and the magnitude of the impedance is more stable towards the explosion (see Fig. 8). In this case, the −0.5° phase threshold exceeded at 56 °C cell temperature. This confirms that the selected frequency for the impedance measurement has little SoC dependency. The first impedance warning is given at 59 °C cell temperature, 12.23 min before the TR. The phase is then stabilized at around −1.05 °C at 89 °C cell temperature. At this SoC, the gas sensor does not measure any increase in the gas concentration until the cell has vented, at 176 °C cell temperature, 2.21 min before the TR. Finally, the second impedance warning is given at 100 °C, 8.15 min before the TR, well before the gas sensor warning. The minimum of the impedance magnitude takes place at 83 °C cell temperature, a little lower than at 100 % SoC. All in all, the impedance behaves very similarly to the 100 % SoC test, although the time window for early detection is larger than at 100 % SoC. However, the gas sensor decreases its reliability, due to the lower amount of gases released by the cell at lower SoC levels [52]. As for the undervoltage, the warning is given 3.66 min prior to the explosion.

3.3. Module Thermal Runaway results

The TR event at module level is carried out with all cells charged to 100 % SoC (see Fig. 9). Although this event should be very similar to the 100 % SoC single cell event, it is slower in time. At single cell events, the heater was directly attached to the DUT, with no other elements for thermal conductivity. At module level, the mass surrounding the heater is greater, so the heat is distributed differently. Hence, this event resembles more a TR event that could happen in a real application. The −0.5° impedance phase threshold is exceeded at 52 °C cell temperature, and the first impedance warning is given at 55 °C cell temperature, 16.79 min before the TR. The phase continued to drop until stabilizing at 82 °C, at a value around −1.65°, a little more than the single cell event. The second impedance warning is given at 93 °C cell temperature, 11.27 min before the TR. As for the gas sensor, in this case, as opposed to the previous single cell tests, it performs better and starts measuring an increase in the gas concentration far before. The sensor gives the first and second warnings 9.67 min and 7.71 min before the explosion

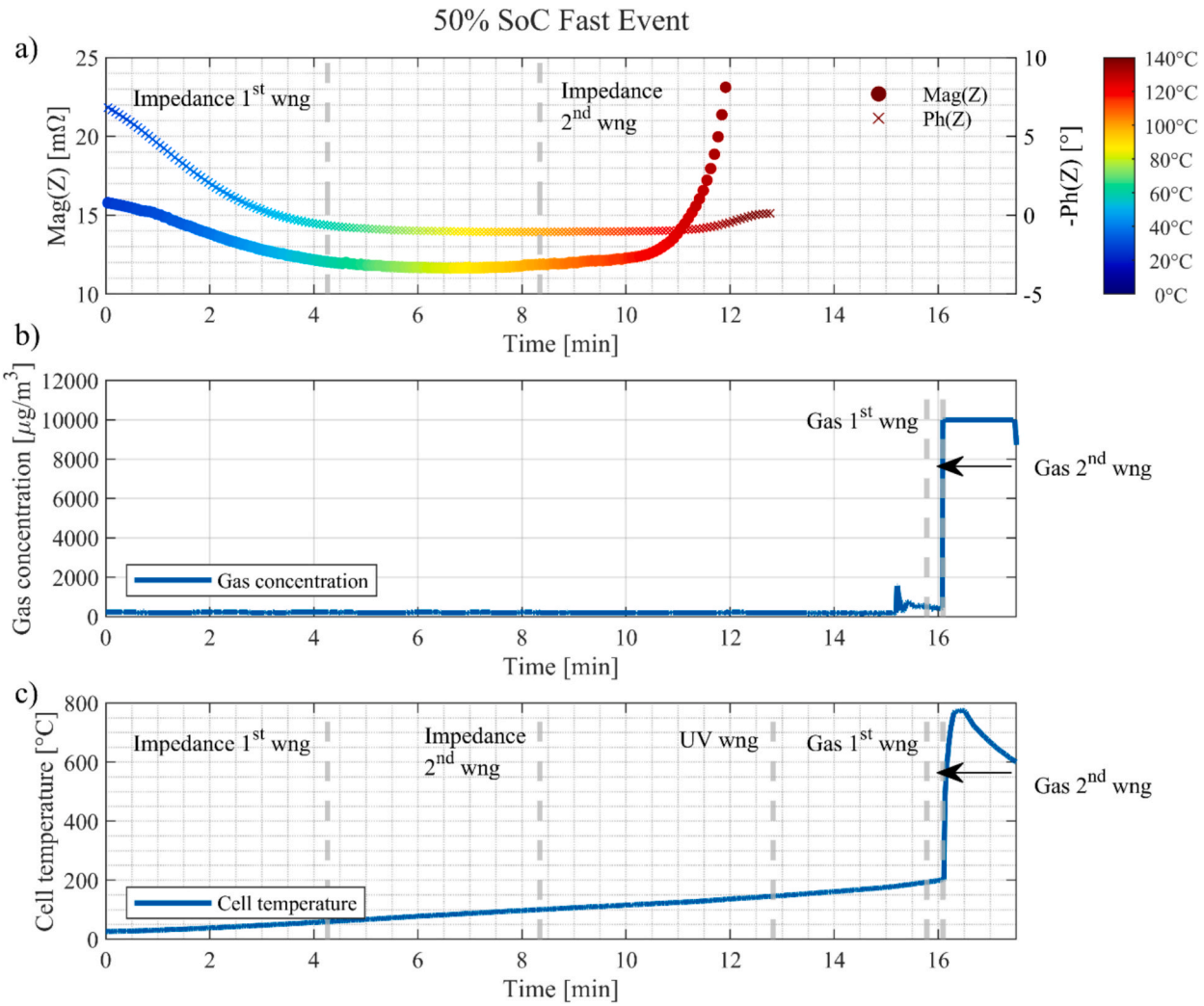

Fig. 8. Fast event results at Test No. 5, 50% SoC OVT test. a) Impedance magnitude and phase evolution over time at the selected frequency. b) Gas concentration evolution. c) Cell temperature evolution during the Thermal Runaway.

respectively, above the 5-minute threshold. The undervoltage warning is given 3.77 min before the explosion in this case. The random behavior of the temperature at the end are caused by the thermocouples becoming loose due to the explosion.

3.4. Comparison between impedance and gas sensor detection

Once both tests have been described, and the results from impedance and gas measurements have also been analyzed, a comparison between both warning methods and the differences due to the cell's SoC level is carried out. It must be noted that gas sensors were excluded from ARC tests due to the temperature limitations of the gas sensor's electronics. As a result, a direct comparison between gas sensing and impedance-based detection could not be performed under slow-paced TR conditions, but have been rather compared during fast-paced over-temperature testing. The results of the EIS-based warning method and the gas sensor warning method demonstrate a clear difference in both timing and performance. The impedance-based method consistently gave warnings earlier than the gas sensors in both SoC conditions. This detection approach offers the potential to detect hazardous internal temperature changes long before gas emissions become evident. In Fig. 10, the effectiveness of each warning is observed for the three tests carried out, where the warning time prior to the TR is shown. Furthermore, the numerical results of the warning times and temperatures can be found in Table A 1 and Table A 2 in the Annex.

At 100 % SoC, the impedance-based method provides a first warning more than 6 min before the explosion and more than 4 min before the gas sensor gives its first warning. However, the imminent TR warning difference between the impedance-based method and the gas sensor is just 52 s. This showcases that although the EIS-based detection method is superior in performance to the gas sensor for early-stage detection, gas sensors may still provide useful confirmation in later stages of a TR and could potentially offer a redundancy in the detection system. As for the 50 % SoC case, the impedance-based method outperformed significantly the gas sensor. The EIS provides both warnings more than 5 min before the explosion, while the gas sensor just signals the warning less than a minute prior to the TR. The SoC level dramatically affects the responsiveness of the gas sensor, while the impedance tracking is enhanced due to the increased time to TR. The larger time window for early detection at lower SoC levels highlights the better performance of the impedance tracking, where less energy is stored, the internal chemical reactions due to overtemperature take place at a slower rate and thus the cell's internal material changes are more easily tracked through impedance shifts. Although it was not possible to test the gas sensors at slow-paced TR conditions, this behavior would remain the same. At higher SoC levels, due to the slow heating of the cell, the warning times of the gas sensor and the impedance would be much closer than at fast-paced events. As for lower SoC levels, the same limitation found at fast-paced events would apply to the gas sensor, making it underperform against the impedance-based detection approach. In addition to the SoC

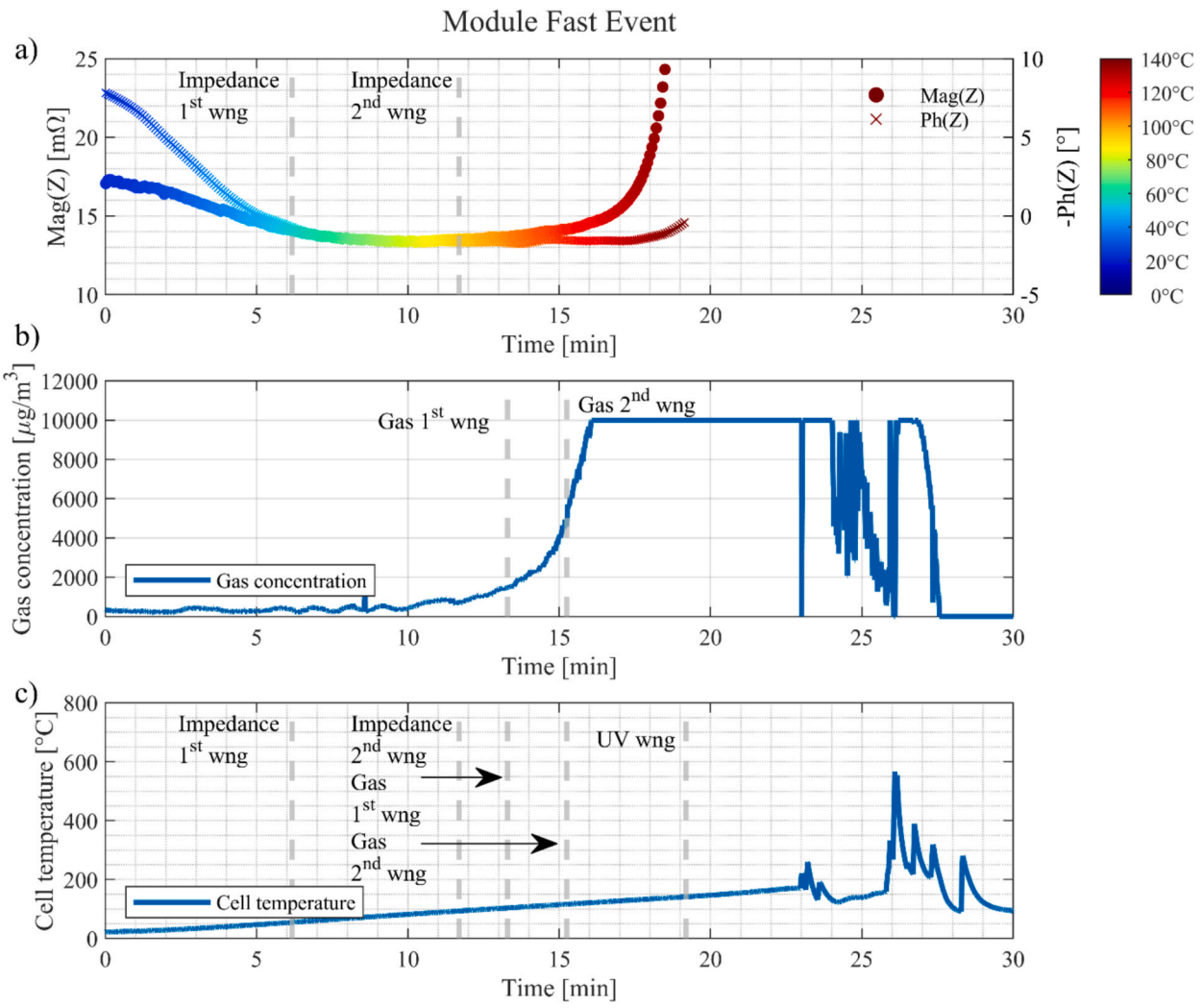

Fig. 9. Fast event results at module level at Test No. 6, 100% SoC module OVT test. a) Impedance magnitude and phase evolution at the selected frequency of the overheated cell. b) Gas concentration evolution. c) Cell temperature evolution of the overheated cell during the Thermal Runaway.

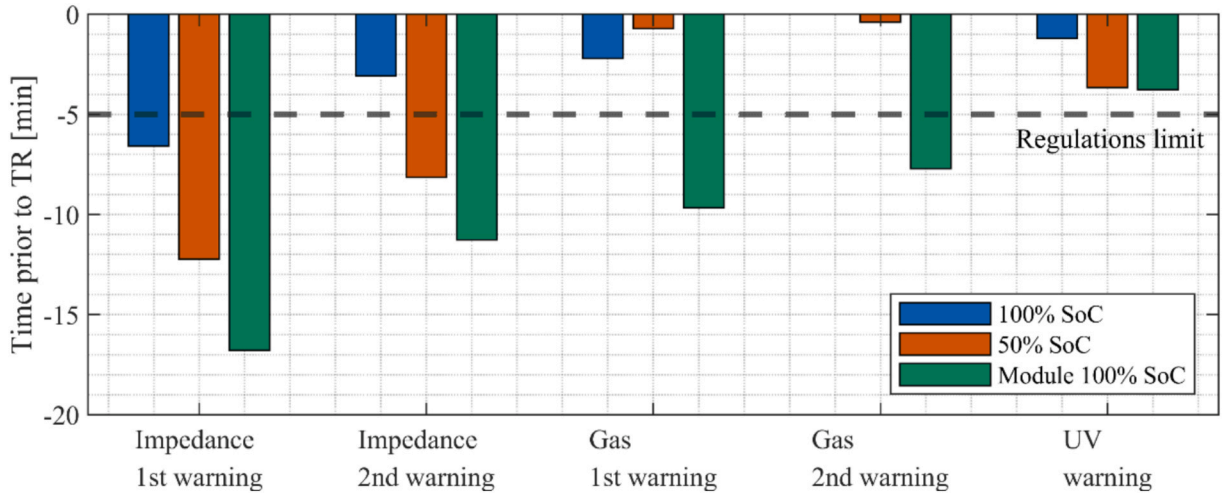

Fig. 10. Comparison of warning times for the different detection approaches during the 3 fast event tests.

variable, the gas sensor's warning is also affected by the number of gas sensors, their position and how the gas flow takes place within the battery pack, not studied in this work. Switching the focus to a module/pack level application, there is a possibility for the EIS hardware to become damaged when the first cell enters TR. The gas sensors can also provide an increased redundancy level to the system's safety level in this

case.

Overall, the earlier detection capabilities of the EIS method can be attributed to its ability to monitor internal cell conditions directly through impedance changes, while gas sensors rely on detecting the byproducts of decomposition of the cell's material caused by overheating. As previously discussed, since the reliability of the gas sensor detection framework depends greatly on geometrical aspects of the battery pack, its performance can greatly diminish in fast-paced events. Furthermore, the EIS-based method demonstrated to give early warnings consistently regardless of the cell's SoC level, with the phase shift proving to be a reliable indicator of early thermal instability. These facts underscore the potential of EIS for real-time TR monitoring in fast-paced overtemperature triggered TR scenarios. Nonetheless, at slower paced events, the gas sensor can also be useful and provide redundancy from a system level point of view, providing an increased level of safety to the overall system and application.

4. Conclusion

This study presents an impedance-based TR early detection methodology for lithium-ion batteries, leveraging single-frequency EIS measurements for tracking cell changes due to temperature. The methodology has been validated in slow-paced events (ARC) and fast-paced events (overtemperature) at cell and module level, comparing its effectiveness to current market solutions, such as gas sensors.

The results confirm that the proposed impedance-based methodology provides significantly earlier warning times than automotive-grade gas sensors. In slow-paced events, the last warning is given approximately 15 h before the explosion. In fast-paced events (under 20 min), the impedance monitoring provided a warning between 6 and 12 min before the explosion. In contrast, the gas sensor only detected the event 2 min before the explosion at 100 % SoC and no detection was achieved for the 50 % SoC before the explosion. This performance highlights the potential of impedance-based strategies as an effective method for TR detection for complying with the 5-minute regulation requirement, such as in the R100 Rev3.

A key advantage of the proposed methodology is the high level of reliability it offers regardless of the SoC level. The results show that the impedance-based strategy ensures consistent detection performance across different levels of SoC. In contrast, gas sensors proved to be less reliable at lower SoC levels due to the reduced amount of gas released during the event. This methodology also demonstrates strong potential for practical implementation in BMS. Numerous studies have shown that EIS is an accurate tool for detecting TR. However, one limitation of using a single chip per BMS is the need for multiplexing, required to monitor cells individually. This can create time gaps where a cell undergoing TR may not be monitored. In this case, this technique requires only one impedance measurement IC per battery module or per battery pack. Hence, this is a cost-effective and minimally invasive solution for large-scale adoption. Furthermore, this approach analyzes the impedance changes qualitatively instead of quantitatively. This technique provides robustness to the detection framework, since it is not subject to the influence of the wiring, connection resistance and so on. Gas sensing solutions can also be implemented in the required application for improving the system's overall redundancy level. The drawback of the proposed methodology is that to find the best frequency, the impedance characterization should be performed to each new cell. Although fixing a specific frequency to target the SEI processes could be valid for TR detection, for achieving the largest detection time possible, the full characterization must be carried out.

Future work will focus on evaluating this methodology across different battery chemistries, formats, degradation levels and abuse mechanisms. One line of work will be to evaluate the performance derating of this methodology across the battery's lifespan when the impedance is just characterized at BoL. The second line of work will be to characterize the cell impedance at different states of degradation, until EoL, to confirm if the proposed strategy can be adjusted with the estimated SoH of the cell to enhance the overall performance.

CRediT authorship contribution statement

J. Perez: Writing – review & editing, Writing – original draft, Investigation, Methodology, Conceptualization. **E. Garayalde:** Writing – review & editing, Writing – original draft, Conceptualization. **J. Lorente:** Writing – review & editing, Conceptualization. **M. Arrinda:** Writing – review & editing, Conceptualization. **M. Oyarbide:** Writing – review & editing, Conceptualization. **H. Macicior:** Writing – review & editing, Supervision. **U. Iraola:** Writing – review & editing, Conceptualization. **H.J. Grande:** Supervision.

Declaration of competing interest

The authors declare that they have no known competing financial interests or personal relationships that could have appeared to influence the work reported in this paper.

Acknowledgments

This work was supported by the EU funded Horizon Europe program (Grant Agreement No. 101137975) under the InnoBMS project. Views and opinions expressed are however those of the author(s) only and do not necessarily reflect those of the European Union. Neither the European Union nor the granting authority can be held responsible for them.

Appendix

Table A1
Warning times prior to Thermal Runaway. Negative values are prior to the TR, positive values are post TR.

SoC	Level	Impedance 1st warning	Impedance 2nd warning	Gas 1st warning	Gas 2nd warning	UV warning
100 %	Cell	−6,58 min	−3,08 min	−2,21 min	0,00 min	−1,21 min
50 %	Cell	−12,23 min	−8,15 min	−0,71 min	−0,40 min	−3,66 min
100 %	Module	−16,79 min	−11,27 min	−9,67 min	−7,71 min	−3,77 min
100 %	ARC	−18,87 h	−15.28 h	N/A	N/A	−9.81 h

Table A2
Temperatures at which the warnings are given during the abusive tests. Gas measurements are not applicable for the ARC test.

SoC	Level	Impedance 1st warning	Impedance 2nd warning	Gas 1st warning	Gas 2nd warning	UV warning
100 %	Cell	54,00 °C	99,00 °C	113,53 °C	252,88 °C	130,59 °C
50 %	Cell	59,00 °C	100,00 °C	193,11 °C	201,89 °C	145,76 °C
100 %	Module	55,00 °C	93,00 °C	103,52 °C	116,05 °C	141,36 °C
100 %	ARC	76,00 °C	98,00 °C	N/A	N/A	121,84 °C

Data availability

Data will be made available on request.

References

[1] Zhang G, Wei X, Tang X, Zhu J, Chen S, Dai H. Internal short circuit mechanisms, experimental approaches and detection methods of lithium-ion batteries for electric vehicles: a review. Renew Sustain Energy Rev 2021;141. https://doi.org/10.1016/j.rser.2021.110790.

[2] Shahid S, Agelin-Chaab M. A review of thermal runaway prevention and mitigation strategies for lithium-ion batteries. Energy Convers Manage: X 2022;16:100310. https://doi.org/10.1016/j.ecmx.2022.100310.

[3] Wang D, Zheng L, Li X, Du G, Zhang Z, Feng Y, et al. Effects of overdischarge rate on thermal runaway of NCM811 Li-ion batteries. Energies (Basel) 2020;13. https://doi.org/10.3390/en13153885.

[4] Chen X, Li L, Liu M, Huang T, Yu A. Detection of lithium plating in lithium-ion batteries by distribution of relaxation times. J Power Sources 2021;496. https://doi.org/10.1016/j.jpowsour.2021.229867.

[5] Shen Y, Wang X, Jiang Z, Luo B, Chen D, Wei X, et al. Online detection of lithium plating onset during constant and multistage constant current fast charging for lithium-ion batteries. Appl Energy 2024;370. https://doi.org/10.1016/j.apenergy.2024.123631.

[6] United Nations Economic Commission for Europe (UNECE), UNECE R100 Rev.3, 2022.

[7] United Nations Economic Commission for Europe (UNECE), UNECE GTR-EVS No.20: Global Technical Regulation on the Electric Vehicle Safety (EVS), 2018.

[8] National Standard of the People's Republic China (GB), GB 38031-2020 Electric Vehicles traction battery safety requirements, 2020.

[9] International Electrotechnical Commission (IEC), IEC 62933-5-2:2020. Electrical energy storage (EES) systems - Part 5-2: Safety requirements for grid-integrated EES systems - Electrochemical-based systems, 2020.

[10] Kong D, Lv H, Ping P, Wang G. A review of early warning methods of thermal runaway of lithium ion batteries. J Energy Storage 2023;64:107073. https://doi.org/10.1016/J.EST.2023.107073.

[11] Raghavan A, Kiesel P, Sommer LW, Schwartz J, Lochbaum A, Hegyi A, et al. Embedded fiber-optic sensing for accurate internal monitoring of cell state in advanced battery management systems part 1: cell embedding method and performance. J Power Sources 2017;341:466–73. https://doi.org/10.1016/J.JPOWSOUR.2016.11.104.

[12] Ganguli A, Saha B, Raghavan A, Kiesel P, Arakaki K, Schuh A, et al. Embedded fiber-optic sensing for accurate internal monitoring of cell state in advanced battery management systems part 2: internal cell signals and utility for state estimation. J Power Sources 2017;341:474–82. https://doi.org/10.1016/j.jpowsour.2016.11.103.

[13] T. Cai, S. Pannala, A.G. Stefanopoulou, J.B. Siegel, Battery Internal Short Detection Methodology Using Cell Swelling Measurements, in: 2020 American Control Conference (ACC), 2020: pp. 1143–1148. doi: 10.23919/ACC45564.2020.9147956.

[14] Kwak E, Son DS, Jeong S, Oh KY. Characterization of the mechanical responses of a LiFePO4 battery under different operating conditions. J Energy Storage 2020;28:101269. https://doi.org/10.1016/J.EST.2020.101269.

[15] Koch S, Birke KP, Kuhn R. Fast thermal runaway detection for lithium-ion cells in large scale traction batteries. Batteries 2018;4. https://doi.org/10.3390/batteries4020016.

[16] Essl C, Seifert L, Rabe M, Fuchs A. Early detection of failing automotive batteries using gas sensors. Energies MDPI 2020. https://doi.org/10.3390/batteries.

[17] Appleberry MC, Kowalski JA, Africk SA, Mitchell J, Ferree TC, Chang V, et al. Avoiding thermal runaway in lithium-ion batteries using ultrasound detection of early failure mechanisms. J Power Sources 2022;535:231423. https://doi.org/10.1016/J.JPOWSOUR.2022.231423.

[18] A. Bombik, S.Y. Sara Ha, M. Faisal Haider, A. Nasrollahi, F.-K. Chang, Li-ion Battery Health Estimation Using Ultrasonic Guided Wave Data and an Extended Kalman Filter, in: 2021 IEEE Applied Power Electronics Conference and Exposition (APEC), 2021: pp. 962–966. doi: 10.1109/APEC42165.2021.9487367.

[19] Zhang G, Cao L, Ge S, Wang C-Y, Shaffer CE, Rahn CD. In situ measurement of radial temperature distributions in cylindrical Li-Ion cells. J Electrochem Soc 2014;161:A1499. https://doi.org/10.1149/2.0051410jes.

[20] Lee CY, Lee SJ, Hung YM, Te Hsieh C, Chang YM, Huang YT, et al. Integrated microsensor for real-time microscopic monitoring of local temperature, voltage and current inside lithium ion battery. Sens Actuators A Phys 2017;253:59–68. https://doi.org/10.1016/J.SNA.2016.10.011.

[21] Forgez C, Vinh Do D, Friedrich G, Morcrette M, Delacourt C. Thermal modeling of a cylindrical LiFePO4/graphite lithium-ion battery. J Power Sources 195 2010:2961–8. https://doi.org/10.1016/J.JPOWSOUR.2009.10.105.

[22] Su T, Lyu N, Zhao Z, Wang H, Jin Y. Safety warning of lithium-ion battery energy storage station via venting acoustic signal detection for grid application. J Energy Storage 2021;38:102498. https://doi.org/10.1016/J.EST.2021.102498.

[23] Lyu N, Jin Y, Miao S, Xiong R, Xu H, Gao J, et al. Fault warning and location in battery energy storage systems via venting acoustic signal. IEEE J Emerg Sel Top Power Electron 2023;11:100–8. https://doi.org/10.1109/JESTPE.2021.3101151.

[24] Shen H, Wang H, Li M, Li C, Zhang Y, Li Y, et al. Thermal runaway characteristics and gas composition analysis of lithium-ion batteries with different LFP and NCM cathode materials under inert atmosphere. Electronics (Switzerland) 2023;12. https://doi.org/10.3390/electronics12071603.

[25] Ren D, Feng X, Liu L, Hsu H, Lu L, Wang L, et al. Investigating the relationship between internal short circuit and thermal runaway of lithium-ion batteries under thermal abuse condition. Energy Storage Mater 2021;34:563–73. https://doi.org/10.1016/j.ensm.2020.10.020.

[26] Straßer A, Adam A, Li J. In operando detection of Lithium plating via electrochemical impedance spectroscopy for automotive batteries. J Power Sources 2023;580:233366. https://doi.org/10.1016/j.jpowsour.2023.233366.

[27] Spinner NS, Love CT, Rose-Pehrsson SL, Tuttle SG. Expanding the operational limits of the single-point impedance diagnostic for internal temperature monitoring of lithium-ion batteries. Electrochim Acta 2015;174:488–93. https://doi.org/10.1016/j.electacta.2015.06.003.

[28] Raijmakers LHJ, Danilov DL, Van Lammeren JPM, Lammers MJG, Notten PHL. Sensorless battery temperature measurements based on electrochemical impedance spectroscopy. J Power Sources 2014;247:539–44. https://doi.org/10.1016/j.jpowsour.2013.09.005.

[29] Raijmakers LHJ, Danilov DL, Van Lammeren JPM, Lammers TJG, Bergveld HJ, Notten PHL. Non-zero intercept frequency: an accurate method to determine the integral temperature of Li-Ion batteries. IEEE Trans Ind Electron 2016;63:3168–78. https://doi.org/10.1109/TIE.2016.2516961.

[30] Jiang D, Zhang Y, Gao Z, Zhang Z, Li S, Jin Y, et al. Single frequency feature point derived from DRT for SOH estimation of lithium ion battery. J Electrochem Soc 2025;172:30514. https://doi.org/10.1149/1945-7111/adbc24.

[31] Keilhofer J, Adam Dorau F, Hsiao H-C, Suthar B, Daub R. Method—impedance modeling of lithium plating during fast charging of lithium-ion cells to derive monitoring strategies. J Electrochem Soc 2024;171:110520. https://doi.org/10.1149/1945-7111/ad92dc.

[32] Kim J, Krüger L, Kowal J. On-line state-of-health estimation of Lithium-ion battery cells using frequency excitation. J Energy Storage 2020;32:101841. https://doi.org/10.1016/j.est.2020.101841.

[33] Kong L, Fang S, Niu T, Chen G, Yang L, Liao R. Fast State of charge estimation for lithium-ion battery based on electrochemical impedance spectroscopy frequency feature extraction. IEEE Trans Ind Appl 2024;60:1369–79. https://doi.org/10.1109/TIA.2023.3324632.

[34] A. Samanta, A. Huynh, N. Shrestha, S. Williamson, Combined data driven and online impedance measurement-based lithium-ion battery state of health estimation for electric vehicle battery management systems, in: 2023 IEEE Applied Power Electronics Conference and Exposition (APEC), 2023: pp. 862–866. doi: 10.1109/APEC43580.2023.10131471.

[35] Srinivasan R, Demirev PA, Carkhuff BG. Rapid monitoring of impedance phase shifts in lithium-ion batteries for hazard prevention. J Power Sources 2018;405. https://doi.org/10.1016/j.jpowsour.2018.10.014.

[36] Dong P, Liu Z, Wu P, Li Z, Wang Z, Zhang J. Reliable and early warning of lithium-ion battery thermal runaway based on electrochemical impedance spectrum. J Electrochem Soc 2021;168:090529. https://doi.org/10.1149/1945-7111/ac239b.

[37] Cai T, Stefanopoulou AG, Siegel JB. Early detection for Li-ion batteries thermal runaway based on gas sensing. ECS Trans 2019;89:85–97. https://doi.org/10.1149/08901.0085ecst.

[38] Dahn JR, Fuller EW, Obrovac M, von Sacken U. Thermal stability of LixCoO2, LixNiO2 and λ-MnO2 and consequences for the safety of Li-ion cells. Solid State Ion 1994;69:265–70. https://doi.org/10.1016/0167-2738(94)90415-4.

[39] Iurilli P, Brivio C, Wood V. On the use of electrochemical impedance spectroscopy to characterize and model the aging phenomena of lithium-ion batteries: a critical review. J Power Sources 2021;505:229860. https://doi.org/10.1016/j.jpowsour.2021.229860.

[40] Mc Carthy K, Gullapalli H, Ryan KM, Kennedy T. Review—use of impedance spectroscopy for the estimation of Li-ion battery state of charge, state of health and

internal temperature. J Electrochem Soc 168 2021:080517. https://doi.org/10.1149/1945-7111/ac1a85.
[41] Haussmann P, Melbert J. Internal cell temperature measurement and thermal modeling of lithium ion cells for automotive applications by means of electrochemical impedance spectroscopy. SAE Int J Alt Power 2017;6. https://doi.org/10.4271/2017-01.
[42] Schmidt JP, Arnold S, Loges A, Werner D, Wetzel T, Ivers-Tiffée E. Measurement of the internal cell temperature via impedance: evaluation and application of a new method. J Power Sources 2013;243:110–7. https://doi.org/10.1016/j.jpowsour.2013.06.013.
[43] Zhu JG, Sun ZC, Wei XZ, Dai HF. A new lithium-ion battery internal temperature on-line estimate method based on electrochemical impedance spectroscopy measurement. J Power Sources 2015;274:990–1004. https://doi.org/10.1016/j.jpowsour.2014.10.182.
[44] Feng X, Ouyang M, Liu X, Lu L, Xia Y, He X. Thermal runaway mechanism of lithium ion battery for electric vehicles: a review. Energy Storage Mater 2018;10:246–67. https://doi.org/10.1016/j.ensm.2017.05.013.
[45] He T, Zhang T, Gadkari S, Wang Z, Mao N, Cai Q. An investigation on thermal runaway behaviour of a cylindrical lithium-ion battery under different states of charge based on thermal tests and a three-dimensional thermal runaway model. J Clean Prod 2023;388:135980. https://doi.org/10.1016/j.jclepro.2023.135980.
[46] Menz F, Bauer M, Böse O, Pausch M, Danzer MA. Investigating the thermal runaway behaviour of fresh and aged large prismatic lithium-ion cells in overtemperature experiments. Batteries 2023;9. https://doi.org/10.3390/batteries9030159.
[47] Andre D, Meiler M, Steiner K, Wimmer Ch, Soczka-Guth T, Sauer DU. Characterization of high-power lithium-ion batteries by electrochemical impedance spectroscopy. I experimental investigation. J Power Sources 2011;196:5334–41. https://doi.org/10.1016/j.jpowsour.2010.12.102.
[48] Srinivasan R, Carkhuff BG, Butler MH, Baisden AC. Instantaneous measurement of the internal temperature in lithium-ion rechargeable cells. Electrochim Acta 2011;56:6198–204. https://doi.org/10.1016/j.electacta.2011.03.136.
[49] Ma R, He J, Deng Y. Investigation and comparison of the electrochemical impedance spectroscopy and internal resistance indicators for early-stage internal short circuit detection through battery aging. J Energy Storage 2022;54. https://doi.org/10.1016/j.est.2022.105346.
[50] Kong X, Plett GL, Scott Trimboli M, Zhang Z, Qiao D, Zhao T, et al. Pseudo-two-dimensional model and impedance diagnosis of micro internal short circuit in lithium-ion cells. J Energy Storage 2020;27. https://doi.org/10.1016/j.est.2019.101085.
[51] Koleti UR, Dinh TQ, Marco J. A new on-line method for lithium plating detection in lithium-ion batteries. J Power Sources 2020;451. https://doi.org/10.1016/j.jpowsour.2020.227798.
[52] Liao Z, Zhang S, Li K, Zhao M, Qiu Z, Han D, et al. Hazard analysis of thermally abused lithium-ion batteries at different state of charges. J Energy Storage 2020;27. https://doi.org/10.1016/j.est.2019.101065.

Glossary

ARC: Accelerated Rate Calorimeter
BMS: Battery Management System
BoL: Beginning of Life
CMU: Cell Monitoring Unit
DEC: Diethyl Carbonate
DMC: Dimethyl Carbonate
DUT: Device Under Test
EIS: Electrochemical Impedance Spectroscopy
EMC: Ethyl Methyl Carbonate
EoL: End of Life
EV: Electric Vehicle
HWS: Heat Wait Seek
IC: Integrated Circuit
LFP: Lithium Iron Phosphate
LIB: Lithium-Ion Battery
LTO: Lithium Titanate
NCA: Nickel Cobalt-Aluminum Oxide
NMC: Nickel Manganese Cobalt Oxide
OVT: Overtemperature
SEI: Solid Electrolyte Interphase
SOA: Safety Operating Area
SoC: State-of-Charge
SoH: State-of-Health
SoS: State-of-Safety
TR: Thermal Runaway
VOC: Volatile Organic Compounds